

BRISTOL UNIV (ENGLAND)

DATA

BRISTOL UNIV (ENGLAND)
GLASS FIBRE/EPOXY RESIN INTERFACE LIFE-TIME PREDICTION.(U)

MAR 82 K H ASHBEE, N R FARRAR, J P SARGENT

DAJA37-81-C-0214

NL

UNCLASSIFIED

108

2000

100%

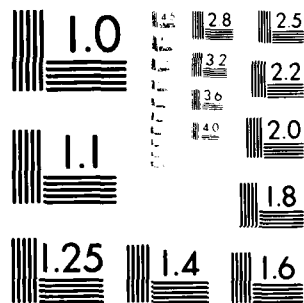
END

DATE

FILMED

00 00

DTIC



MICROCOPY RESOLUTION TEST CHART
NATIONAL BUREAU OF STANDARDS-1963-A

12

UNCLASSIFIED

SECURITY CLASSIFICATION OF THIS PAGE (When Data Entered)

REPORT DOCUMENTATION PAGE		READ INSTRUCTIONS BEFORE COMPLETING FORM
1. REPORT NUMBER	2. GOVT ACCESSION NO.	3. RECIPIENT'S CATALOG NUMBER
	AD A116356	6
4. TITLE (and Subtitle) Glass Fibre/Epoxy Resin Interface Life-Time Prediction		5. TYPE OF REPORT & PERIOD COVERED Annual Technical Report March 1982
		6. PERFORMING ORG. REPORT NUMBER
7. AUTHOR(s) K.H.G. Ashbee J.P. Sargent N.R. Farrar Elizabeth Walter		8. CONTRACT OR GRANT NUMBER(s) DAJA37-81-C-0214
9. PERFORMING ORGANIZATION NAME AND ADDRESS University of Bristol Royal Fort, Tyndall Avenue Bristol BS8 1TL, UK		10. PROGRAM ELEMENT, PROJECT, TASK AREA & WORK UNIT NUMBERS TT161102BH57-04
11. CONTROLLING OFFICE NAME AND ADDRESS USARDCG-UK Box 65 FPO NY 09510		12. REPORT DATE March 1982
14. MONITORING AGENCY NAME & ADDRESS (if different from Controlling Office)		13. NUMBER OF PAGES 47
		15. SECURITY CLASS. (of this report) Unclassified
		15a. DECLASSIFICATION/DOWNGRADING SCHEDULE
16. DISTRIBUTION STATEMENT (of this Report) Approved for public release; Distribution unlimited		
17. DISTRIBUTION STATEMENT (of the abstract entered in Block 20, if different from Report) DTIC ELECTE S JUN 30 1982 D		
18. SUPPLEMENTARY NOTES		
19. KEY WORDS (Continue on reverse side if necessary and identify by block number) Interfacial lifetime, Optical waveguide, Non Destructive Evaluation, Osmosis, Load transfer, Residual stress		
20. ABSTRACT (Continue on reverse side if necessary and identify by block number) The principle of fibre reinforcement requires load transfer from matrix to fibres. In resin matrix composites it is known, from measurements of mechanical strength, that realisation of load transfer is progressively impaired during water uptake from humid in-service environments. The physical mechanisms responsible for this impairment include the generation of interfacial pressure pockets, the occurrence of which suggests that the optical waveguide behaviour of glass reinforced plastics should be affected		

AD A116356

DTIC FILE COPY

DD FORM 1 JAN 73 1473

EDITION OF 1 NOV 65 IS OBSOLETE
S/N 0102-LF-014-6601

UNCLASSIFIED

SECURITY CLASSIFICATION OF THIS PAGE (When Data Entered)

82

UNCLASSIFIED

SECURITY CLASSIFICATION OF THIS PAGE (When Data Entered)

and might therefore offer a non destructive evaluation technique for monitoring at least one of the causes of mechanical degradation. This possibility has been appraised and experimentally verified.

Two models have been developed and applied to interfacial fracture at pressure pockets attributable to osmosis. Direct photoelastic measurements indicative of load transfer in short fibre composites have been used to test the rates of debonding predicted by the two models.

The net stress across the boundary of the first Wigner cell in a fibre reinforced composite must be zero from which it is inferred that, moving around a fibre, the radial principal stress changes sign several times. The origin of the stress can be differential thermal contraction between fibre and matrix materials during cooling from the resin cure temperature, or inhomogeneous swelling associated with water uptake, or externally applied loads. The number of reversals of sign is determined by the fibre lay-up geometry. In the light of this, interfacial failure is expected to initiate at sites located on the loci of maximum residual radial tension. Also, subsequent propagation of individual pressure pockets is expected to be favoured along these loci rather than around the fibre circumference. The fact that such preferred initiation and propagation are not observed is taken to mean that residual stress is more uniformly distributed than expected. The nature of residual stress generated during resin curing and during water uptake/expulsion has consequently been further investigated.

Accession For	
NTIS GRA&I	<input checked="checked" type="checkbox"/>
DTIC TAB	<input type="checkbox"/>
Unannounced	<input type="checkbox"/>
Justification	
By	
Distribution/	
Availability Codes	
Dist	Avail and/or Special
A	



UNCLASSIFIED

SECURITY CLASSIFICATION OF THIS PAGE(When Data Entered)

TABLE OF CONTENTS

Section	Page
LIST OF FIGURES	5
1. INTRODUCTION	8
2. GRP AS OPTICAL WAVEGUIDE - RDE OF INTERFACE LIFE TIME	10
2.1 Background	10
2.2 Specimen preparation	11
2.3 Experimental results and discussion	11
3. OSMOSIS IN COMPOSITE MATERIALS	12
3.1 Hypothesis	12
3.2 Model 1	13
3.3 Model 2	15
3.4 Observations	16
4. ON THE ASSUMPTION THAT EPOXY RESINS ARE FREE FROM MOLECULAR STRESS DURING CURE	17
4.1 Hypothesis	17
4.2 Experimental	17
4.3 Results and Discussion	18
5. THE IRREVERSIBILITY OF DIMENSIONAL CHANGES IN EPOXY RESINS UNDERGOING UPTAKE AND EXPULSION OF WATER	21
5.1 Previous work	21
5.2 Experimental method	21
5.3 Results	21
6. REFERENCES	23
7. PUBLICATIONS, CONFERENCES, SUMMER SCHOOLS	23

LIST OF FIGURES

1. Ray diagram for an optical waveguide
2. Apparatus for manufacture of CR waveguide
3. Optical waveguide test on CR. Flow of light directed through fiber in epoxy resin. $\lambda = 6328$. Composite immersed in distilled water at the boiling point
4. Epiglass/epoxy composite after 20 hrs immersion in boiling water. Specimen viewed between crossed polars (photo developed by M. Vardian)
5. Change in Phase of Polarization During swelling associated with water uptake at 100°C by two epoxy resin alone
6. After van't Hoff (1966) (1)
7. Photoacoustic modulated caused by pressure pulses on the surface of a graphite fiber in an epoxy matrix composite after 400 hrs immersion in distilled water at 40°C
8. Applied stress as a function of volume of a crystalline crack
9. Crack volume versus uniaxial pressure for an inflated crack
10. Energy versus volume of an inflated crack
11. Rate and time of liquid transport uptake during water uptake by various resin matrix composites.
(1) Epiglass/polycarbonate 100°C
(2) Second immersion of specimen 1 after heating 100°C
(3) Epiglass (low swelling agent)/polycarbonate 100°C
(4) Epiglass (low swelling agent)/polycarbonate 100°C
(5) Epiglass/polycarbonate 100°C
(6) Epiglass/polycarbonate 100°C
(7) Epiglass/polycarbonate 200°C
(8) Epiglass/epoxy 100°C
(9) Epiglass/polycarbonate 100°C
(10) Epiglass/epoxy 50°C
(11) Epiglass/epoxy 40°C
12. Schematic representation of the optical bench used for optical interference studies of dimensional stability of resin

13. Part of a sequence of interference patterns photographed during the 30 minute soaking period for a glass slide/resin film 150µm thick cover slip sandwich.
14. Moiré fringes (1) generated by superimposition of interference patterns (1) in order to reveal the deformation of the cover slip after reaching the water temperature (15°C). The cover slip was 150µm thick.
15. Moiré fringes generated by superimposition of the cover slip after 5 minutes at the water temperature (15°C) (Figure 1b).
16. Moiré fringes generated by superimposition of the cover slip subjected to buckling deformation for 10 minutes at the water temperature (15°C) (Figure 1c).
17. Moiré fringes generated by superimposition of interference patterns (1) in order to reveal the deformation of the cover slip after reaching the water temperature (15°C). The cover slip was 150µm thick.
18. Moiré fringes generated by superimposition of interference patterns (1) in order to reveal the deformation of the cover slip after reaching the water temperature (15°C). The cover slip was 150µm thick.
19. (a) Part of a sequence of Moiré fringes taken during the 100 water soaking experiment. (b) Part of a sequence of Moiré fringes taken during the 100 water soaking experiment. (c) Part of a sequence of Moiré fringes taken during the 100 water soaking experiment.
20. Moiré fringes generated by superimposition of interference patterns (1) in order to reveal the deformation of the cover slip after reaching the water temperature (15°C). The cover slip was 150µm thick.
21. Moiré fringes generated by superimposition of interference patterns (1) in order to reveal the deformation of the cover slip after reaching the water temperature (15°C). The cover slip was 150µm thick.
22. Moiré fringes generated by superimposition of interference patterns (1) in order to reveal the deformation of the cover slip after reaching the water temperature (15°C). The cover slip was 150µm thick.
23. Moiré fringes generated by superimposition of interference patterns (1) in order to reveal the deformation of the cover slip after reaching the water temperature (15°C). The cover slip was 150µm thick.
24. Moiré fringes generated by superimposition of interference patterns (1) in order to reveal the deformation of the cover slip after reaching the water temperature (15°C). The cover slip was 150µm thick.

25. Schematic diagram to illustrate the changing geometry of the cover slip during swelling of the adhesive in a joint exposed to an aqueous environment. Description follows notation of swelling at the rim of the joint.

26. Graph of the predicted water concentration (C_w/C_0) as a function of fractional distance from the center of the specimen. (, points representing the calculated concentration for positions corresponding to the sectioning plane shown in Figure 25. All values are 1.0.

1. EXPERIMENTAL PROCEDURE

The first step in the experiment was to determine the effect of the concentration of the solution on the rate of reaction. This was done by measuring the time taken for a fixed volume of gas to be evolved at different concentrations of the reactants. The results are shown in Table 1. It can be seen that the rate of reaction increases with increasing concentration of the reactants. This is expected since a higher concentration of reactants leads to a higher frequency of collisions between the reacting particles.

$$\frac{1}{t} = k[A]^m[B]^n$$

$$k = \frac{1}{t[A]^m[B]^n}$$

$$\frac{1}{t} = k[A]^m[B]^n$$

$$\frac{1}{t} = k[A]^m[B]^n$$

Table 1. Results of the experiment.

Concentration of A (mol/l)	Concentration of B (mol/l)	Time taken for gas to evolve (s)
0.1	0.1	100
0.2	0.1	50
0.1	0.2	50
0.2	0.2	25

From the results in Table 1, it can be seen that the rate of reaction is directly proportional to the concentration of A and inversely proportional to the concentration of B.

$$\text{Rate} = k[A]^1[B]^{-1}$$

The overall order of the reaction is 1 + (-1) = 0. This means that the rate of reaction is independent of the concentration of the reactants.

The results of the experiment show that the rate of reaction is directly proportional to the concentration of A and inversely proportional to the concentration of B. This is expected since a higher concentration of A leads to a higher frequency of collisions between the reacting particles, while a higher concentration of B leads to a lower frequency of collisions.

(b) Unsubstantiated _____

1993 - 1994

$$p = \frac{1}{(1 + \frac{1}{2})^2} = \frac{1}{\frac{9}{4}} = \frac{4}{9}$$

[illegible]

(22) 1000000 1000000 1000000 1000000 1000000

• • •

1990

[illegible]

• • •

1. *Phragmites* (common)

[illegible]

1. The first part of the document is a list of names and addresses, which appears to be a directory or a list of contacts. The names are written in a cursive script, and the addresses are listed below them.

but optical magnification was in total annihilation, $(n_1 - n_2) = 10^{-2}$. The refractive index of the glass is close to 1.5 and, for applications where optical transparency is required - say windows for example - manufacturers try to make the refractive index of the coated resin to that of the glass. They rarely succeed and, as often as not the refractive index mismatch is such that the magnification condition is satisfied. The present experiments were conducted not on uncoated compounds manufactured by polymerising epoxy resins but on compounds of that mould, so designed that it supports a controlled flow of polymer. A photograph of the mould with these in position, and with the oil in the cells as in the case, is shown in Figure 2. A better job, perhaps even more successful, is achieved in order to remove all the surface defects due to the casting the added change, by casting the addition and photographing it under a microscope and by casting the addition of more. It is possible to make the surface of the compound in the addition little of the surface. The same experiment was conducted with the addition of more in the same manner.

[illegible][illegible]

1. Будущее - это то, что еще не произошло, но что обязательно произойдет. Будущее - это то, что еще не произошло, но что обязательно произойдет. Будущее - это то, что еще не произошло, но что обязательно произойдет.

Polarising microscopy of very low fibre volume fraction specimens, Figure 4, reveals the occurrence of interfacial pressure pockets during the first 200 hours. During this time, the resin is also undergoing swelling in order to accommodate the diffused water, Figure 5. Before saturation, at around 200 hours, the concentration of diffused water and hence the swelling is (approximately) distributed and this, in turn, introduces compression near the external surface and tension deeper inside the composite. This stress field is superimposed on to that already generated by the differential thermal contraction between matrix and fibre materials during cooling from the resin cure temperature. The cumulative effect of these changing stresses is evidently discontinuous during the initial stages of water uptake.

Each pressure pocket is filled with aqueous solution and the critical angle over the area of contact between it and the fibre is larger than that for contact between resin and fibre. However, the expected propagation of a larger solid angle of light is not realised until continuity of pressure pockets and absence of elastic deformation is established along the whole length of the waveguide, i.e. not until a very much later stage of water uptake (2000 hours in Figure 5).

1.2. COMMENTS ON EXPERIMENTAL OBSERVATIONS

1.2.1. Diffusion

On which depends the nature of the results related to an osmotic pressure, involving a nearly 50% uptake of completely free of aqueous solution of water, placed in water, by it is concluded that the solid walls of the normal fibre pressure is very low. In accordance to the dissolved water, when, upon the introduction of the solution (water), water will enter the matrix up to a certain limit, thereby increasing the pressure on the walls of fibre matrix, resulting in the matrix, owing to the pressure increasing, further uptake of water. This pressure we have termed osmotic pressure, and is represented by σ .

In this regard, it is reasonable to detect small pockets of water (or other solutes) near the interface between the matrix and fibre, and the liquid and water uptake is limited at the interface, and it corresponds to the frequency of osmotic pressure, which is the 100 component, i.e. the and the solid walls of matrix fibres are susceptible to solvent but not to a large osmotic pressure, which is the 100 component, i.e. the osmotic pressure of a small amount of water. This pressure we have termed osmotic pressure, and is represented by σ . The pressure is a function of the water uptake, and is shown in Figure 6.

3.2 Model 1

When formed, each interfacial pocket closely resembles a penny-shaped crack that has grown in a solid tensioned between fixed grips. The overall change in energy is from U_0 , corresponding to the state of strain energy prior to fracture, to $U_0 - U_G$, where the Griffith energy U_G given by the Zener approximation is

$$U_G = \frac{1}{2} \frac{E_1 \sigma_1^2}{(1 + \frac{E_1}{E_2})} ab^2 = \frac{E_1}{2} \frac{\sigma_1^2}{(1 + \frac{E_1}{E_2})} ab^2$$

$\sigma_1 = \sigma_1$ is the tensile stress applied externally and perpendicular to the crack, E is Young's modulus, a and b respectively are the half thickness and radius of the crack. Referring to figure 8, if the interfacial cavity could be closed by application of traction on its wall, the stress σ_c acting across the walls could rise from 0 to σ_1 and, correspondingly, its volume would decrease from V_0 to 0.

The Griffith energy gained by this process would be

$$U_G = \frac{1}{2} \frac{E_1 \sigma_1^2}{(1 + \frac{E_1}{E_2})} ab^2$$

Then

$$U_G = \frac{1}{2} \frac{E_1 \sigma_1^2}{(1 + \frac{E_1}{E_2})} ab^2$$

By making σ_1 a function of the interfacial crack length with zero external stress, the above is invalid. Instead, a function of an internal pressure, and an external pressure $p = \sigma_1$ gives the same U_G , see Figure 9.

$$U_G = \frac{1}{2} \frac{E_1 \sigma_1^2}{(1 + \frac{E_1}{E_2})} ab^2$$

and the elastic stored energy is

$$U_{el} = \frac{1}{2} \frac{E_1 \sigma_1^2}{(1 + \frac{E_1}{E_2})} ab^2$$

$$\text{Therefore } U_G = \frac{1}{2} \frac{E_1 \sigma_1^2}{(1 + \frac{E_1}{E_2})} ab^2$$

$$\text{and } U_{el} = \frac{1}{2} \frac{E_1 \sigma_1^2}{(1 + \frac{E_1}{E_2})} ab^2$$

A solute exerts an osmotic pressure equal to the pressure that would be exerted by a gas having the same number of molecules in a volume equal to that occupied by the solution. Consider a change in volume of the interfacial cavity from V_0 to V_1 resulting from dissolution of n moles of solute.

$$pV = nRT$$

$$\text{The strain energy release} = \int p dV$$

$$= \int \frac{nRT}{V} dV$$

$$= nRT \log_e \frac{(V_0 + V_1)}{V_0}$$

$$= nRT \log_e \frac{p_1}{p_0}$$

p_0 and p are the values of the osmotic pressure corresponding to volumes V_0 and V_1 respectively.

The overall energy $E = E_{\text{gas}} + E_{\text{elastic}}$

$$= nRT \log_e \frac{(V_0 + V_1)}{V_0} + \frac{3}{8\pi} \frac{F V_1^2}{ab^3}$$

This function is sketched in Figure 10.

The value of V_1 corresponding to minimum energy release may be found by differentiation

$$\frac{dE}{dV_1} = nRT \frac{1}{V_0 + V_1} + \frac{3}{4\pi} \frac{F V_1}{ab^3}$$

$$= 0 \text{ when } V_1^2 + V_1 V_0 = \frac{4\pi}{3} ab^3 nRT = 0$$

$$\text{i.e. when } V_1 = \frac{V_0^2}{2} + \sqrt{\frac{V_0^4}{4} + \frac{4\pi}{3} ab^3 nRT}$$

We must take the positive root, hence

$$V_1 = -\frac{V_0}{2} + \sqrt{\frac{4ab^2 nRT}{3E} \left(1 + \frac{3EV_0^2}{16\pi ab^2 nRT} \right)}$$

$$\sim -\frac{V_0}{2} + \sqrt{\frac{4ab^2 nRT}{3E}} \quad \text{for large values of } b$$

3.3 Model 2

Alternatively, interfacial failure due to cracks inflated by osmotic pressure could be modelled as follows. Suppose a constant pressure reservoir supplies the "gas"

$$\text{Energy, } E = -p_1 V_1 + \frac{1}{2} p_1 V_1 = -\frac{1}{2} p_1 V_1$$

$$= -E_{\text{elastic}} = -\frac{2\pi}{3} \frac{p_1^2}{E} ab^2$$

but $E_{\text{surface}} \sim 2\gamma \pi ab$, where γ is the specific surface energy

$$\text{so } E_{\text{total}} = 2\gamma \pi ab - \frac{2\pi}{3} \frac{p_1^2}{E} ab^2$$

$$\frac{\partial E_{\text{total}}}{\partial b} = 2\gamma \pi a - \frac{4\pi}{3} \frac{p_1^2}{E} ab$$

$$= 2\pi a \left(\gamma - \frac{2}{3} \frac{p_1^2}{E} b \right)$$

which is negative if

$$b > \frac{3E\gamma}{2p_1^2} \quad \text{i.e. if } p > \sqrt{\frac{3E\gamma}{2b}}$$

$$\frac{\partial E_{\text{total}}}{\partial a} = 2\gamma \pi b - \frac{2\pi}{3} \frac{p_1^2}{E} b^2 = 2\pi b \left(\gamma - \frac{p_1^2}{3E} b \right)$$

and is negative if $b > \frac{3E\gamma}{p^2}$

$\frac{\partial E}{\partial b}$ total is evidently more negative than $\frac{\partial E}{\partial a}$ total, so the expression

for p_{crit} is taken from the former.

Taking as trial values $E = 3\text{GPa}$, $\gamma = 1\text{J/m}^2$ and $b = 10\mu\text{m}$,

$$p_{crit} = \sqrt{\frac{3.3 \times 10^9 \cdot 1}{2 \cdot 10^{-5}}} = 10\text{MPa}$$

3.4 Observations

It is important to note the distinctive behaviour of pressure filled interfacial cracks under the two extreme types of inflation outlined in models 1 and 2. Model 2 corresponds to the uniform tensile stress type of loading that was treated by Griffith, and gives rise to an unstable critical crack size such that a smaller crack will not grow while a larger one will grow without limit. This critical crack size corresponds to a maximum in the sum of mechanical and surface energies. Model 1 implies loading at the mouth of the interfacial crack (as by the driving in of a wedge) and results in a stable crack size corresponding to a minimum in the sum of mechanical and gas energies.

Thus, model 2 predicts instantaneous interfacial failure if a constant osmotic pressure equal to a critical pressure can be maintained, whereas model 1 predicts interfacial failure at a rate determined by the requirement that each pressure pocket maintains its volume at a minimum energy level.

In Figure 11, the overall rate of interfacial failure is taken as the rate of loss of load transfer index in short fibre composites. The load transfer index is the optical retardation measured through diameters close to the centre of an individual short fibre minus the optical retardation measured through diameters near the ends of the same fibre. It is evident that interfacial failure proceeds at a rapidly decelerating rate such as would be expected if model 2 dominates at the time of initiation but gives way to model 1 during propagation.

According to model 1, interfacial pressure pockets maintain their volumes at values determined by the square root of the number of moles of dissolved solute. It has been observed that solutes can be leached from the fibre in some cases⁽⁴⁾, leaving an 'etched' fibre surface, and in such cases the availability of the solute is presumably governed by the rate of diffusion of the solute to the surface of the fibre. The simplest diffusion model predicts dependence on the square root of time, and the combination of these two processes leads to a dependence of the volume of the interfacial pressure-filled cavities on the fourth root of time. The broken line in Figure 11 corresponds to a $(\text{time})^{1/4}$ law.

4. ON THE ASSUMPTION THAT EPOXY RESINS ARE FREE FROM SHEAR STRESS DURING CURE

4.1 Hypothesis

The accelerated cure reactions that take place during the elevated temperature curing of epoxy resins promote cross-linking and thereby give rise to shrinkage. There are no superimposed dimensional changes attributable to such processes as chain scissioning, as could be the case in polyesters that contain diffused water, or to the release of volatiles, as might be the consequence of condensation reactions in polyamides for example. The shrinkage is assumed to be homogeneous because any tendency to create shear stress is thought to be relieved by viscoelastic flow. This assumption is based on the premise that before it gels, the fluid resin behaves in a Newtonian fashion and is unable to support shear stress.

4.2 Experimental

19mm diameter soda-lime glass cover slips of two different thicknesses were bonded to 1mm thick soda-lime glass microscope slides. The cover slip thicknesses were 140 μ m and 230 μ m respectively and, the epoxy adhesive was Redux 312/5. The cover slips and microscope slides were thoroughly cleaned by ion bombardment before manufacturing the joints. Each specimen was mounted in a specimen chamber so that the free surface of the cover slip was in close proximity to an optical flat. This assembly was then mounted on an optical bench. In order that a uniform temperature distribution was maintained across the specimen, it was mounted on a thick disc of copper. This in turn was held in good thermal contact with the aluminium specimen chamber. Figure 12 is a schematic diagram of the optical components. The space between cover slip and optical flat is made small enough to allow optical interference between light incident upon and reflected from the free surface of the cover slip. Any changes in shape of the interference cavity, due to deformation of the cover slip caused by non-uniform changes in dimensions of the epoxy layer, cause the pattern of interference fringes to change.

Figure 13 shows a sequence of interference photographs recorded during the warm up period of a specimen manufactured with a 140 μ m thick cover slip. The time taken for the specimen to reach the cure temperature was 30 minutes and a substantial amount of the shape change occurred during this heating-up period. Initially, the cover slip is slightly deformed convex upwards but this soon gives way to a much larger concave deformation, the subsequent development of which is further examined in Figure 14 by creating Moiré patterns between successive photographs of the interference pattern and the pattern photographed when the specimen had completed its half hour cure. The Moiré fringes are the circumferential fringes, each

of which is the locus of points that have suffered identical displacement normal to the joint. The normal displacement of adjacent loci differ by half a wavelength.

4.3 Results and Discussion

Figure 15 shows the normal displacement at different points across a diameter of the same specimen after 5 minutes at the cure temperature, where $t_0 = 30$ minutes is the total time at the cure temperature. The sign of the displacement field was established by applying an identical positive pressure to the cover slip. The curve fits the parabola

$$w = .071 (x - .0095)^2$$

where w is the normal displacement and x is the distance measured from the edge of the specimen

To a first approximation, the deformation of the cover slip can be regarded as identical to that of a circular membrane, rigidly supported at its edge and subjected to a pressure drop (p) across its surfaces. For such a membrane, Love⁽⁵⁾ has shown that the fourth differential of the normal displacement is a measure of p . The cover slip is thin. If thin enough for Love's analysis to be applied, then

$$\nabla^4 w = 0 \text{ when } p = 0$$

Since the data presented in Figure 15 is described by a parabola, the fourth differential $\nabla^4 w / \Delta x^4$ and hence the normal stress σ_{zz} are evidently zero.

Hence it is concluded that the deformation presented in Figure 15 is caused by radial stresses transmitted from the resin to the cover slip and not the stresses created normal to the joint. To check that curing really does cause the parallel sided disc of resin to transform into a concave lens shape, a specimen was manufactured using cover slips for both adherends. As expected, curing caused this sandwich to deform into a double concave lens as might have been produced by the application of edge tractions.

The analogy to the buckling of a thin circular plate simply supported around its edge and subjected to a uniformly distributed edge force applied in the plane of the plate, has been used to estimate the radial stress in the specimen shown in Figure 13.

The relations between the strains, displacements and stresses as given by Stoker (6) are

$$\epsilon_{xx} = \frac{\partial u}{\partial x} + \frac{1}{2} \left(\frac{\partial w}{\partial x} \right)^2 = \sigma_{xx} / E$$

$$\epsilon_{xy} = \frac{1}{2} \left(\frac{\partial u}{\partial y} + \frac{\partial v}{\partial x} \right) = \tau_{xy} / E$$

$$\epsilon_{yy} = \frac{\partial v}{\partial y} + \frac{1}{2} \left(\frac{\partial w}{\partial y} \right)^2 = \sigma_{yy} / E$$

where the u, v, w components of the displacement of a point on the middle surface of the plate are denoted by u, v, w respectively.

The middle surface stresses divided by the modulus of elasticity E are denoted by $\sigma_{xx}, \sigma_{yy}, \tau_{xy}$ and the middle surface strains by $\epsilon_{xx}, \epsilon_{yy}, \epsilon_{xy}$.

Since we assume radial symmetry, we may put $\sigma_{xx} = \sigma_{yy}$ and making the approximation that $\partial u / \partial x$ is sufficiently small relative to $1/2(\partial w / \partial x)^2$ such that it may be neglected gives

$$\frac{1}{2} \left(\frac{\partial w}{\partial x} \right)^2 = \sigma_{xx} (\nu + 1)$$

where ν = Poisson's ratio.

Figure 15 shows the distribution of stress $\sigma_{xx} = \tau_{xy}$ obtained using the above equation for the deformation shown in Figure 14.

The above estimate is based on a deformation which is wholly elastic. An alternative estimate, using a simple viscoelastic model, is as follows. The raw adhesive film has a larger thermal expansion coefficient than glass. During heating to the cure temperature, the resin is free to expand in the thickness direction but radially it has to work against viscosity and its velocity relative to the glass is zero or close to zero at contact, becoming progressively larger at deeper layers. As a consequence, the cover slip is deformed convex upwards. Approaching the cure temperature, the shrinkage associated with the accelerated cure reaction dominates and the cover slip deformation is reversed to the concave shape sketched in Figure 15. An order of magnitude estimate of the in-plane shear stresses is obtained as follows. The adhesive layer is 150 μ m thick and 19mm in diameter, so the ratio of unrestricted in-plane shrinkage to thickness shrinkage is

$$= 150 \times 10^{-6} / 9.5 \times 10^{-3} = 1.58 \times 10^{-2}$$

[illegible]

١٥

- 0001-2-02-000**

1. The first group of respondents (Group 1) consisted of 100 individuals who were randomly selected from the population of 1,000 individuals. The second group (Group 2) consisted of 100 individuals who were randomly selected from the population of 1,000 individuals. The third group (Group 3) consisted of 100 individuals who were randomly selected from the population of 1,000 individuals. The fourth group (Group 4) consisted of 100 individuals who were randomly selected from the population of 1,000 individuals. The fifth group (Group 5) consisted of 100 individuals who were randomly selected from the population of 1,000 individuals. The sixth group (Group 6) consisted of 100 individuals who were randomly selected from the population of 1,000 individuals. The seventh group (Group 7) consisted of 100 individuals who were randomly selected from the population of 1,000 individuals. The eighth group (Group 8) consisted of 100 individuals who were randomly selected from the population of 1,000 individuals. The ninth group (Group 9) consisted of 100 individuals who were randomly selected from the population of 1,000 individuals. The tenth group (Group 10) consisted of 100 individuals who were randomly selected from the population of 1,000 individuals.

2. C_{10}H_8 (Naphthalene) C_{10}H_6 (Anthracene) C_{10}H_4 (Phenanthrene) C_{10}H_2 (Pyrene) C_{10}H_0 (Benzo[a]pyrene)
 3. $\text{C}_{12}\text{H}_{18}$ (Dodecane) $\text{C}_{12}\text{H}_{16}$ (Dodecene) $\text{C}_{12}\text{H}_{14}$ (Dodecadiene) $\text{C}_{12}\text{H}_{12}$ (Dodecatriene) $\text{C}_{12}\text{H}_{10}$ (Dodecatetraene) C_{12}H_8 (Dodecapentaene) C_{12}H_6 (Dodecahexaene) C_{12}H_4 (Dodecaheptaene) C_{12}H_2 (Dodecaoctaene) C_{12}H_0 (Dodecanonaene)

1. The first group of people who are interested in the results of the study are the researchers themselves. They want to know if the study was successful in achieving its objectives and if the results are consistent with their expectations.

10-11-68

7-10-2000 10:00 AM

1. The first step is to identify the problem or question that needs to be answered. This involves understanding the context and the specific requirements of the task.

¹ The α and β phases of the polymer are separated by a sharp interface which is not visible by light microscopy. The α phase is the more crystalline phase.

² α and β phases are separated by a sharp interface.

³ The α phase is the more crystalline phase.

⁴ The α and β phases of the polymer are separated by a sharp interface which is not visible by light microscopy.

⁵ α and β phases are separated by a sharp interface.

⁶ The α and β phases of the polymer are separated by a sharp interface which is not visible by light microscopy. The α phase is the more crystalline phase.

⁷ The α and β phases of the polymer are separated by a sharp interface which is not visible by light microscopy. The α phase is the more crystalline phase.

⁸ α and β phases are separated by a sharp interface.

⁹ The α and β phases of the polymer are separated by a sharp interface which is not visible by light microscopy.

¹⁰ The α and β phases of the polymer are separated by a sharp interface which is not visible by light microscopy. The α phase is the more crystalline phase.

¹¹ α and β phases are separated by a sharp interface.

¹² The α and β phases of the polymer are separated by a sharp interface which is not visible by light microscopy.

¹³ The α and β phases of the polymer are separated by a sharp interface which is not visible by light microscopy.

¹⁴ α and β phases are separated by a sharp interface.

¹⁵ The α and β phases of the polymer are separated by a sharp interface which is not visible by light microscopy. The α phase is the more crystalline phase.

¹⁶ The α and β phases of the polymer are separated by a sharp interface which is not visible by light microscopy.

¹⁷ α and β phases are separated by a sharp interface.

¹⁸ The α and β phases of the polymer are separated by a sharp interface which is not visible by light microscopy.

¹⁹ The α and β phases of the polymer are separated by a sharp interface which is not visible by light microscopy.

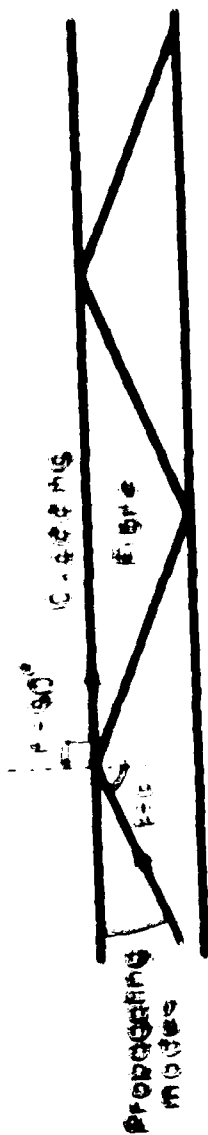
²⁰ The α and β phases of the polymer are separated by a sharp interface which is not visible by light microscopy. The α phase is the more crystalline phase.

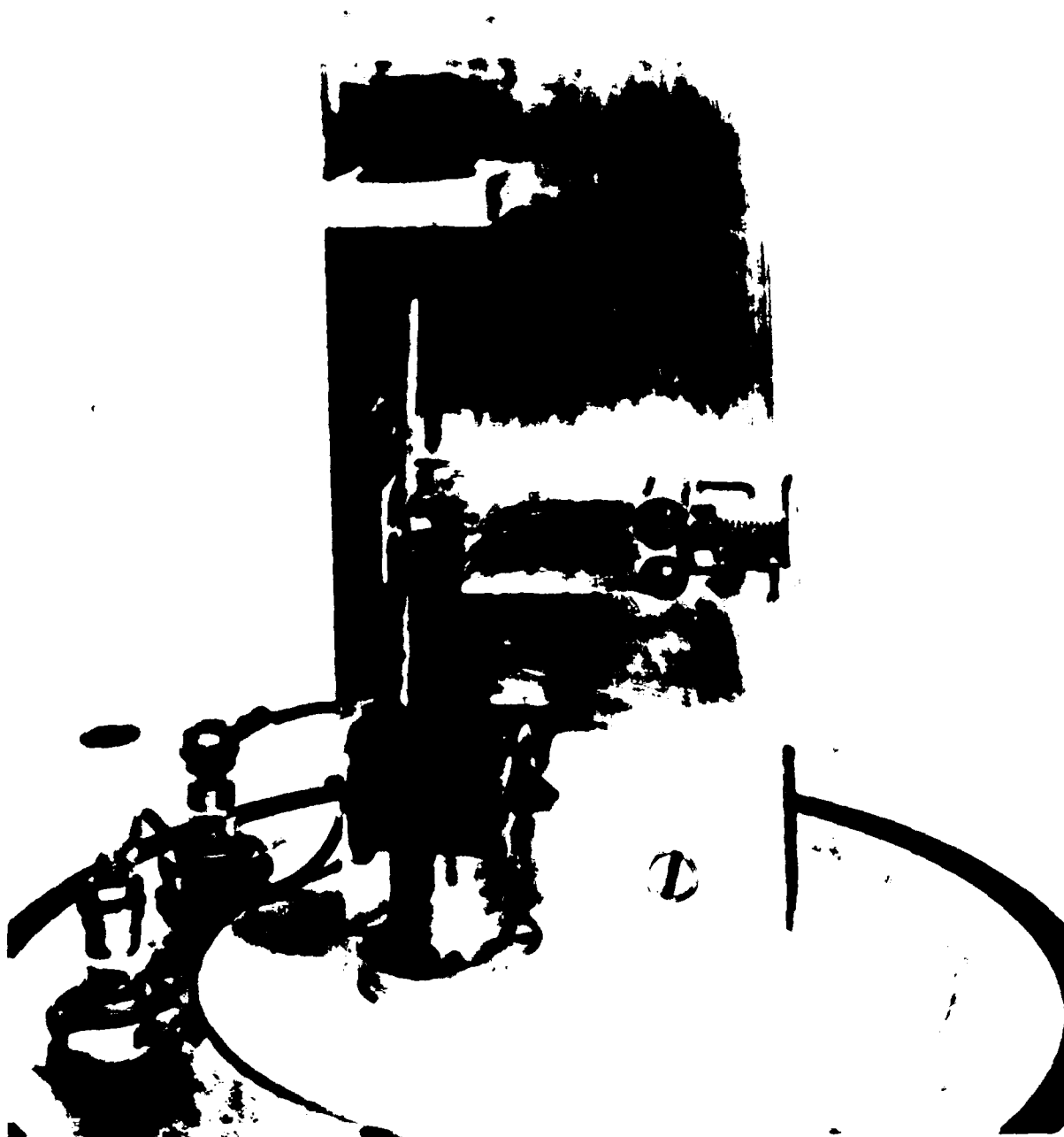
²¹ The α and β phases of the polymer are separated by a sharp interface which is not visible by light microscopy.

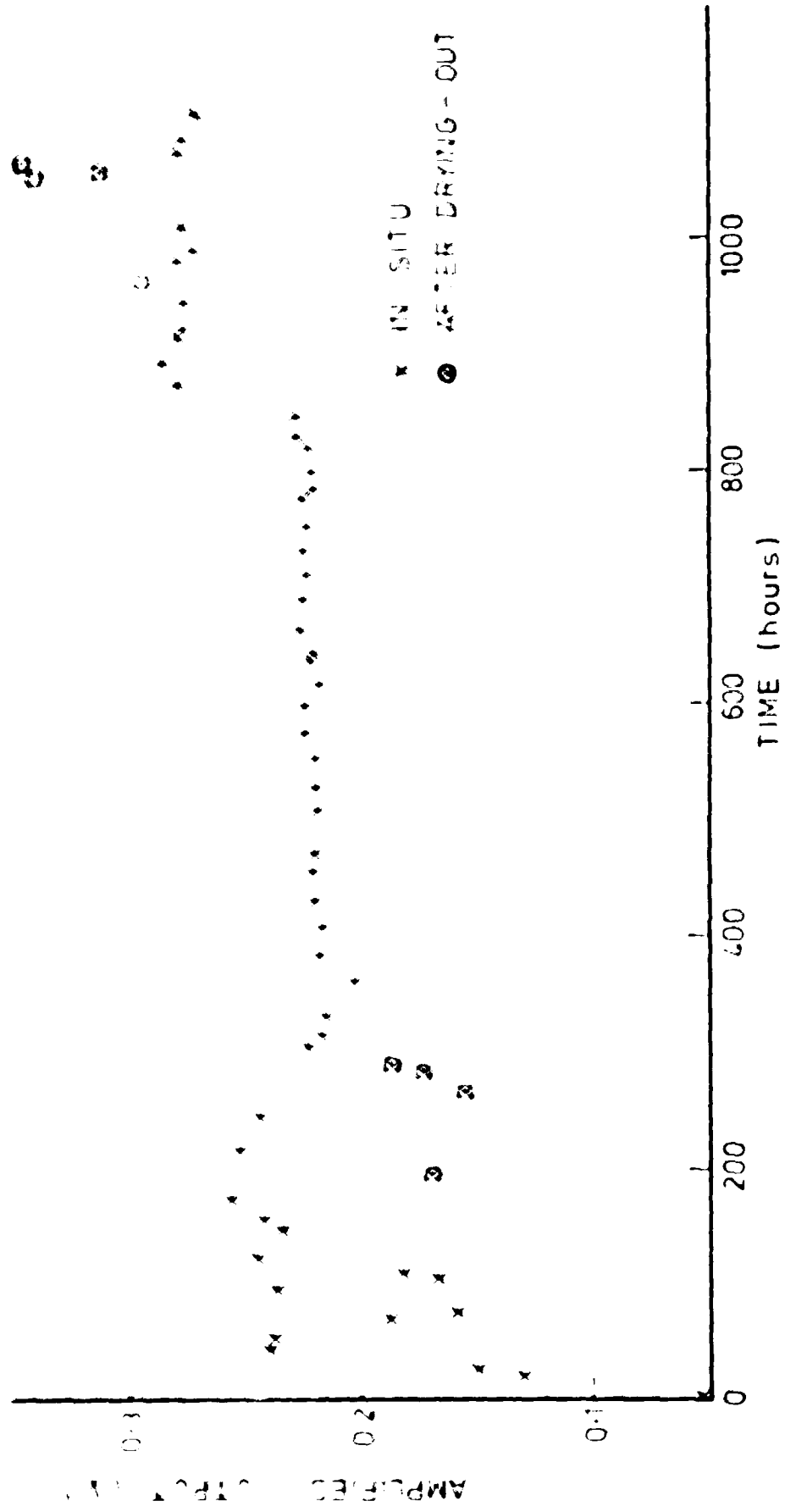
²² The α and β phases of the polymer are separated by a sharp interface which is not visible by light microscopy. The α phase is the more crystalline phase.

²³ The α and β phases of the polymer are separated by a sharp interface which is not visible by light microscopy. The α phase is the more crystalline phase.

²⁴ The α and β phases of the polymer are separated by a sharp interface which is not visible by light microscopy. The α phase is the more crystalline phase.

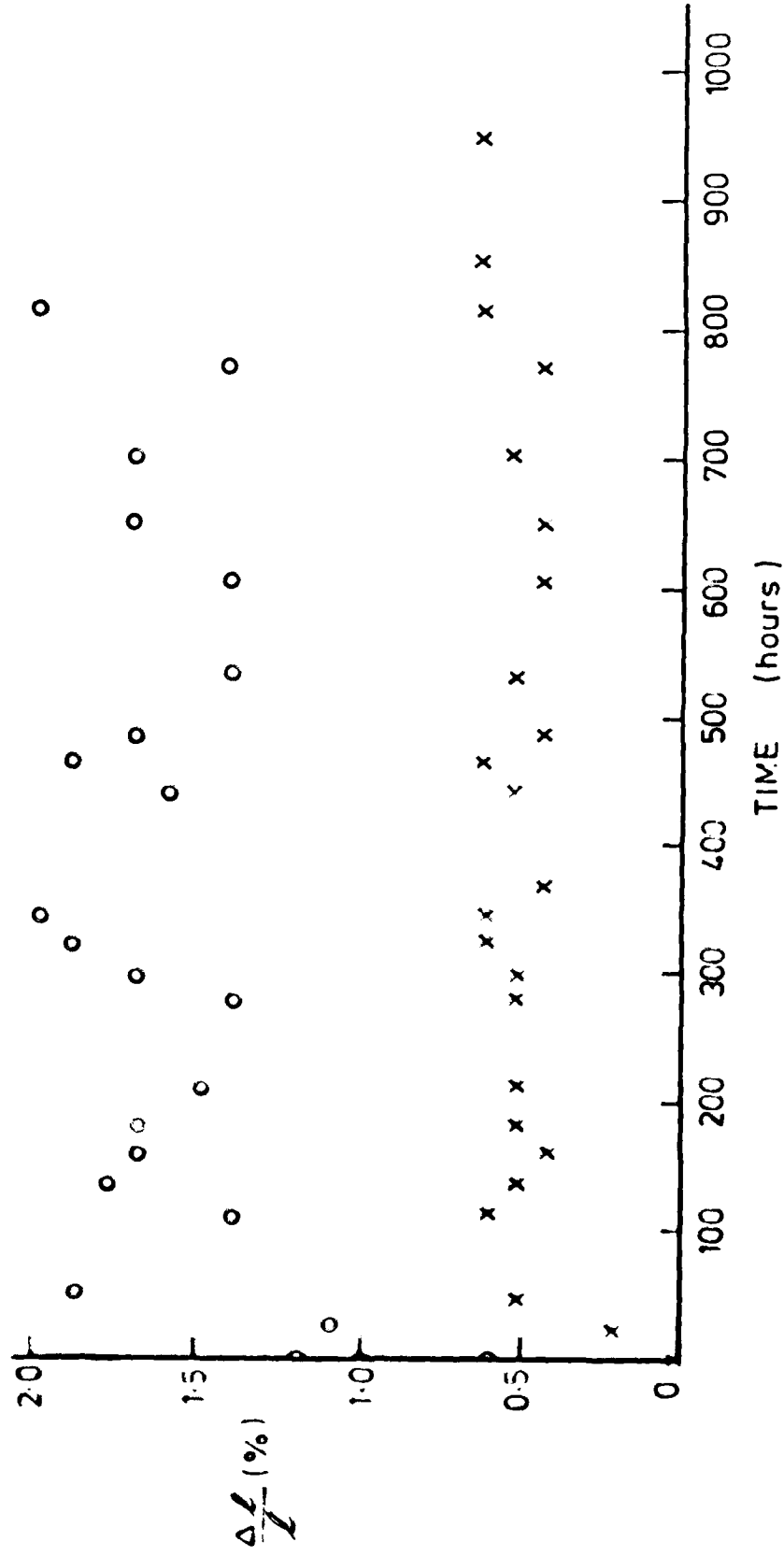




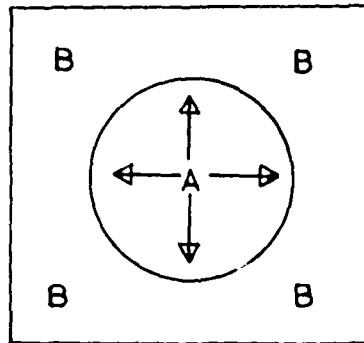


3. Optical density test on EPP. Top of 10m diameter E-glass fibres in epoxy resin. 3 x 10⁶ fibres. Control for 1000h in distilled water at

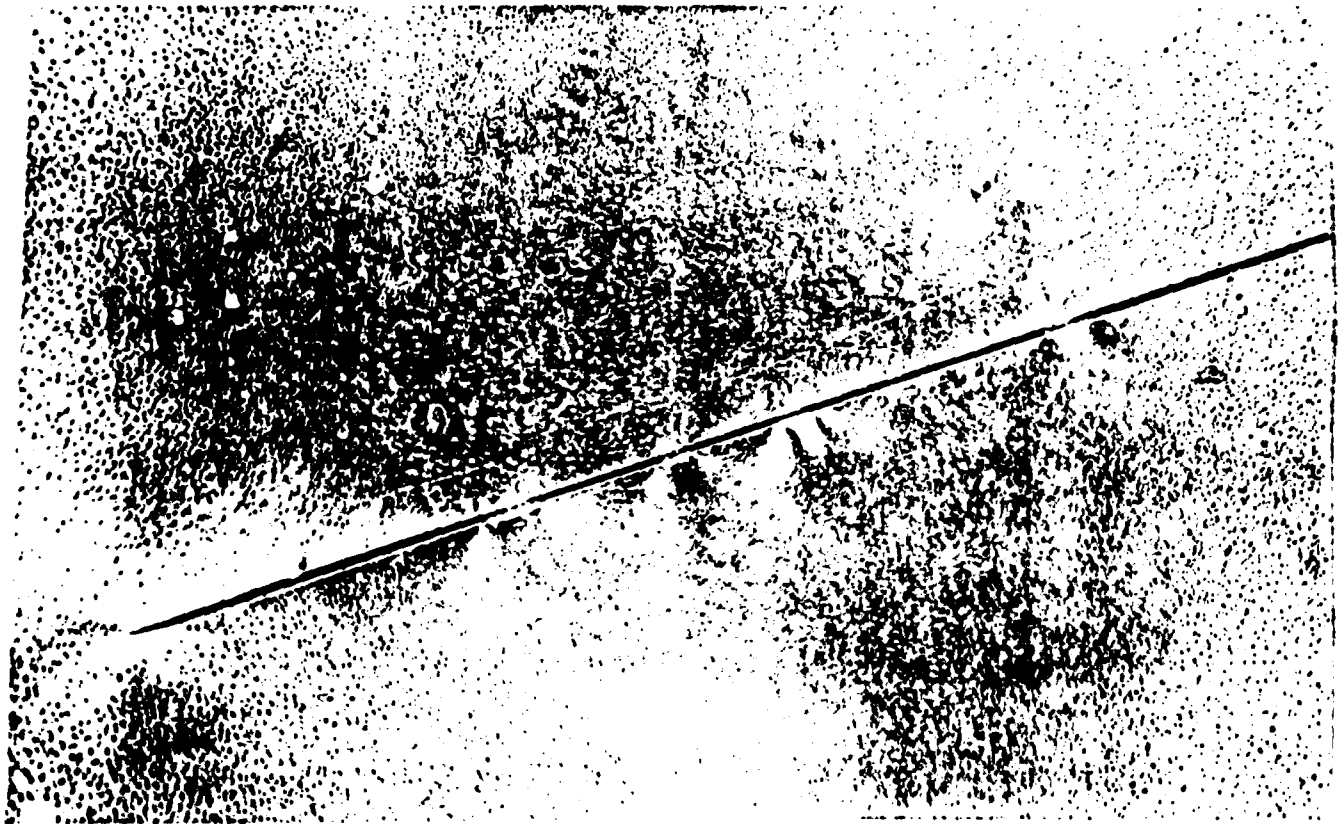




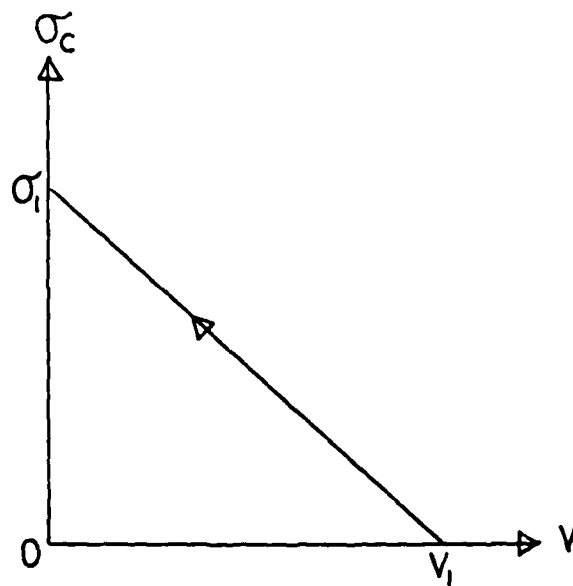
5. Change in linear dimensions during swelling associated with water uptake at 100°C by two epoxy resin slabs



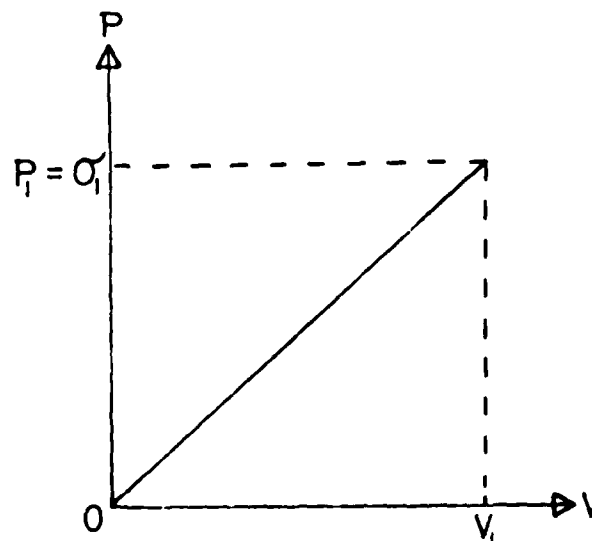
6. After van't Hoff (1888)⁽³⁾



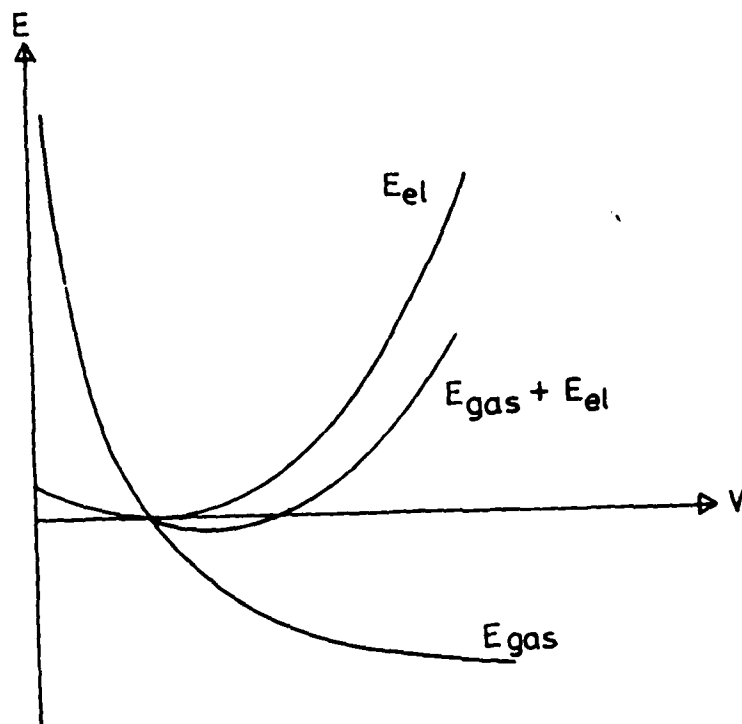
7. Photoelastic contrast caused by pressure pockets on the surface of a graphite fibre in an epoxy matrix composite after 600 hrs immersion in distilled water at 80C



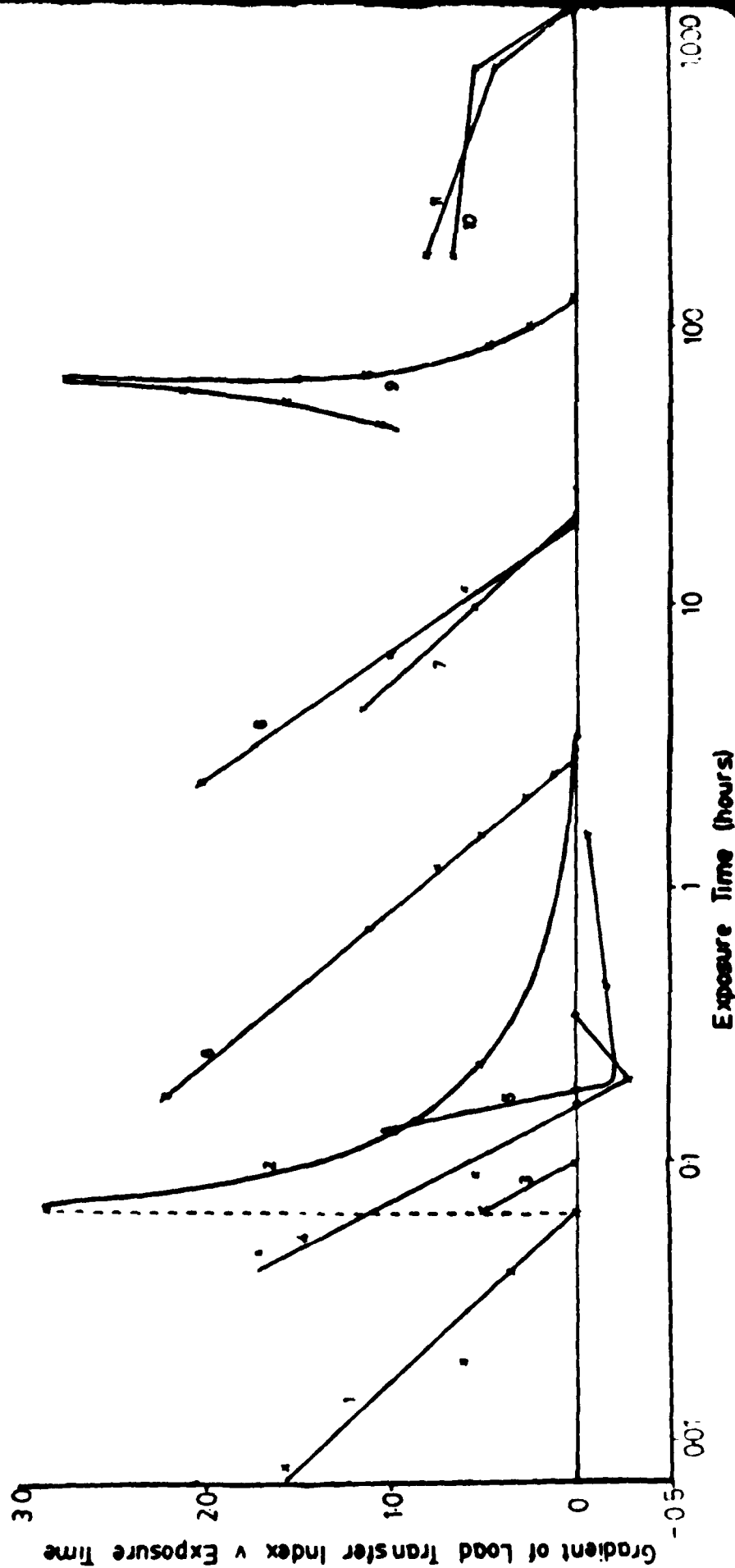
8. Applied stress as a function of volume of a Griffith's crack



9. Crack volume versus internal pressure for an inflated crack

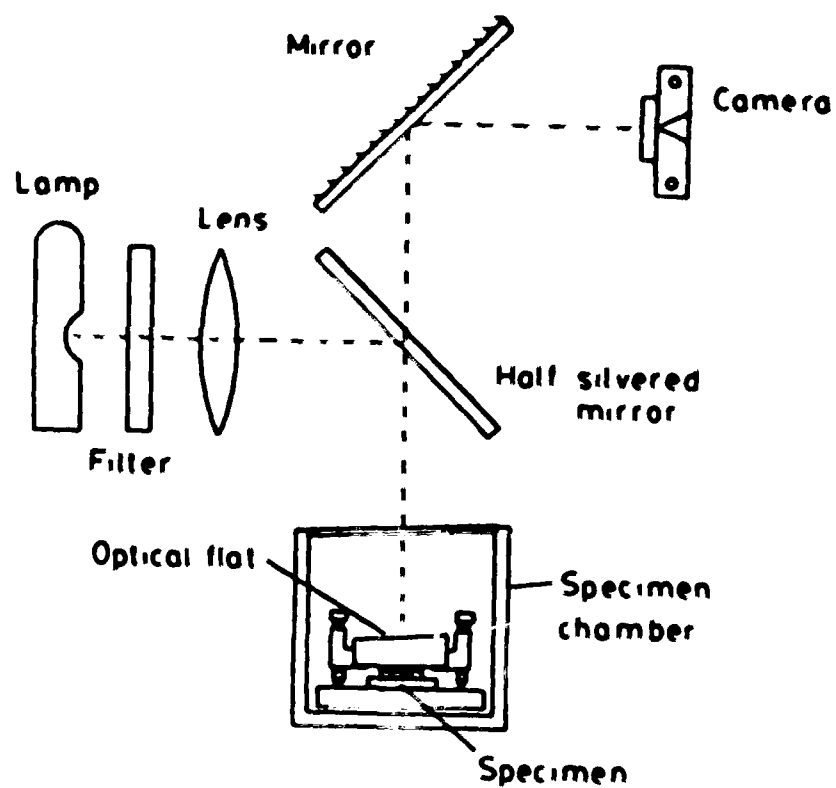


10. Energy versus volume of an inflated crack

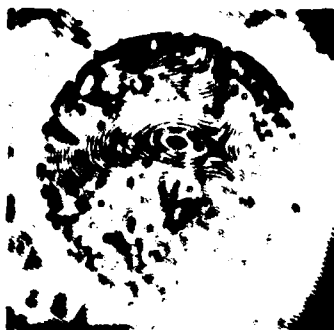


11. Rate of loss of load transfer index during water uptake by various resin matrix composites.

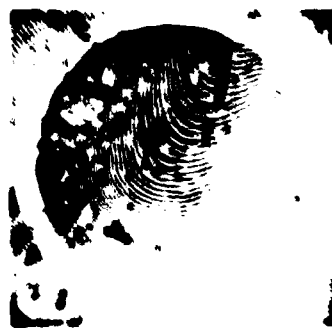
- (1) E-glass/polyester 100C
- (2) Second immersion of specimen 1 after drying 100C
- (3) E-glass (no coupling agent) polyester 100C
- (4) E-glass (no coupling agent) polyester 100C
- (5) E-glass/polyester 100C
- (6) E-glass/polyester 20C
- (7) E-glass/polyester 20C
- (8) E-glass/epoxy 100C
- (9) E-glass/polyester 100C
- (10) S-glass/epoxy 80C
- (11) S-glass/epoxy 80C



12. Schematic representation of the optical bench used for optical interference studies of dimensional stability of resins



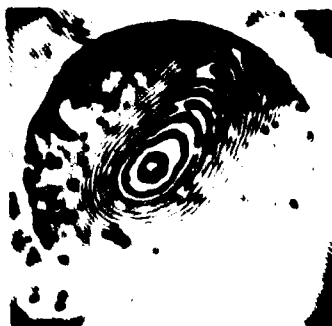
227



228



229



230

13. Part of a sequence of interferometer patterns photographed during the 10 minute warming period for a glass slide/germ film/150 μ m thick cover slip sandwich.



Fig. 1. Micrographs of the superimposition of interference patterns on the surface of the film. The film was 1.5 mm thick.

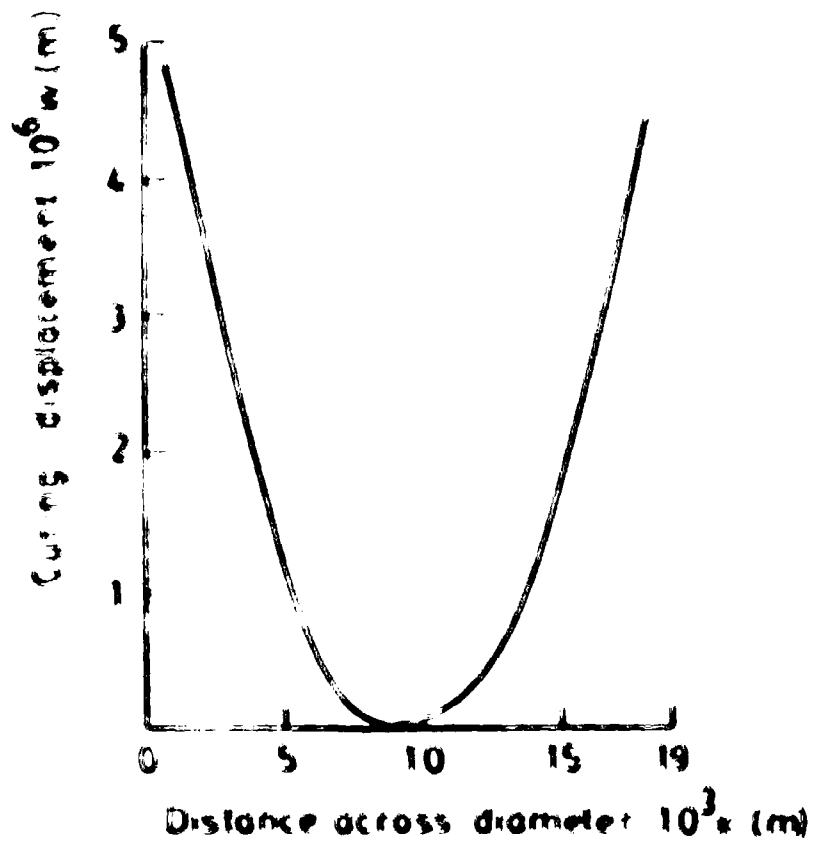
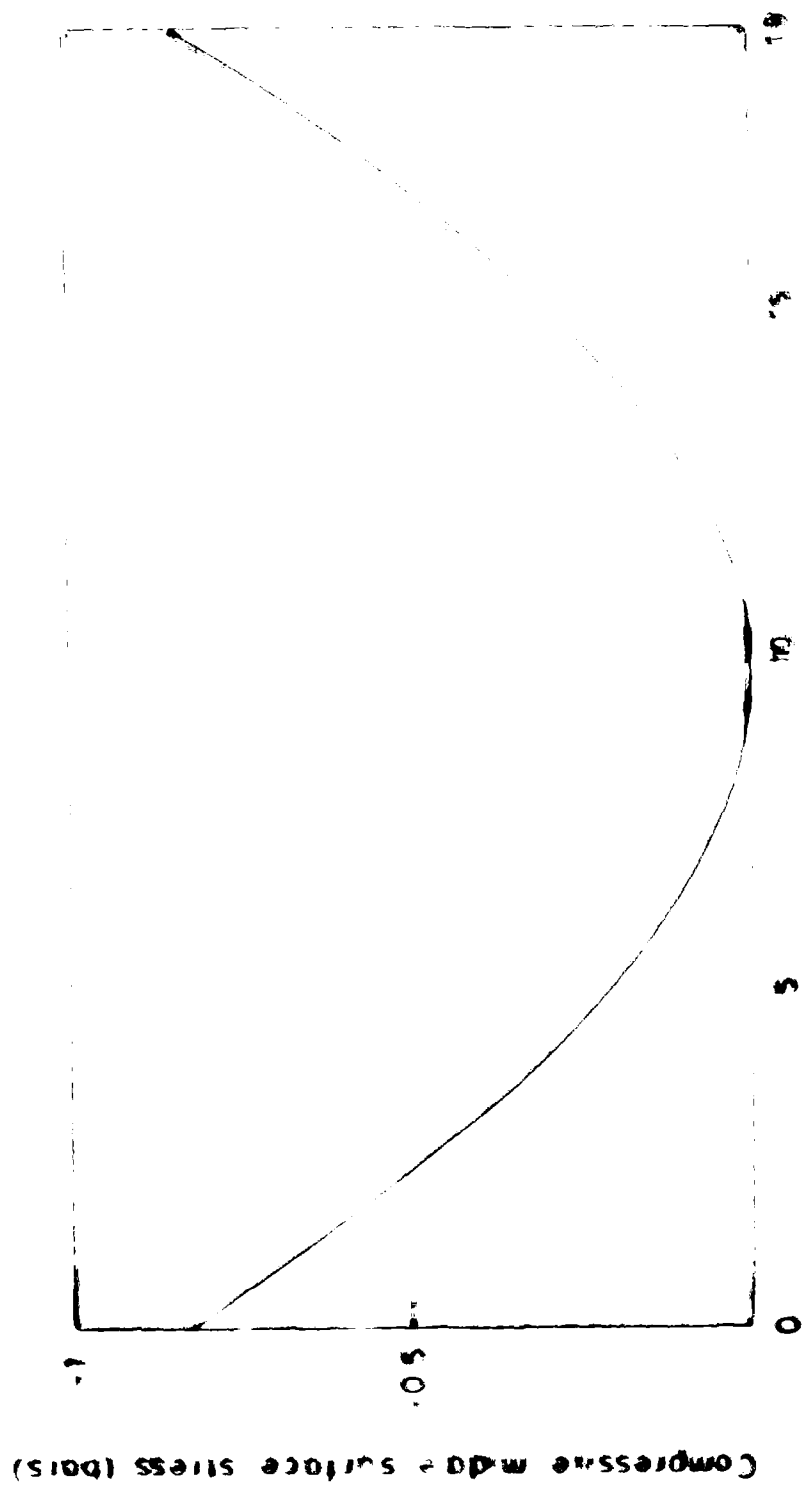


FIG. 1. Curie displacement (m) versus distance across diameter (m) after 5 minutes at 100°C. (Curie displacement, 10⁶ m; distance, 10³ m).



(a) Relationship of stress and distance

14. The following table shows the results of the tests conducted on the specimens of the material under consideration.

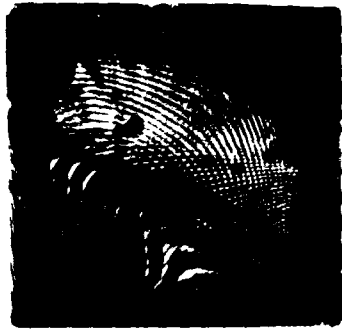
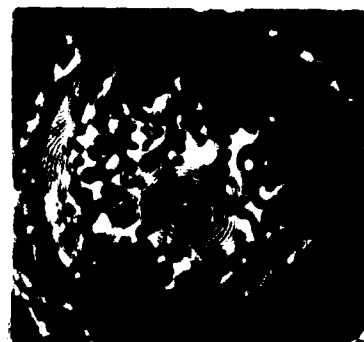


Fig. 1. Micrograph of a cross-section of a biological specimen showing concentric rings. The rings are formed by the deposition of calcium phosphate. The rings are formed by the deposition of calcium phosphate. The rings are formed by the deposition of calcium phosphate.



100x

200x

200x

Fig. 2. Micrograph of a cross-section of a biological specimen showing concentric rings. The rings are formed by the deposition of calcium phosphate. The rings are formed by the deposition of calcium phosphate. The rings are formed by the deposition of calcium phosphate.



Figure 1



Figure 2

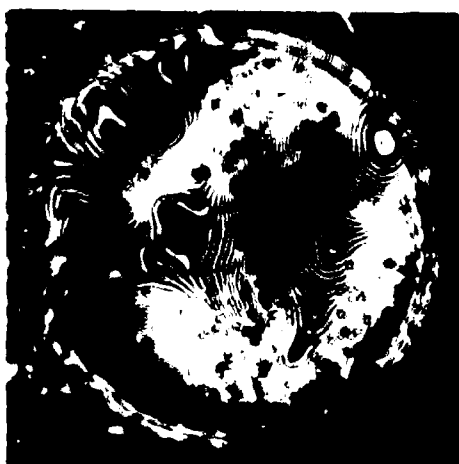


Figure 3

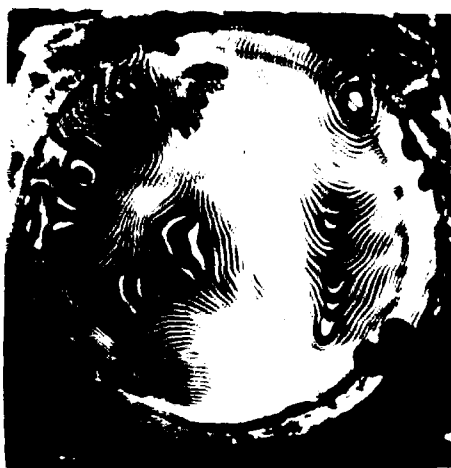


Figure 4



Figure 5

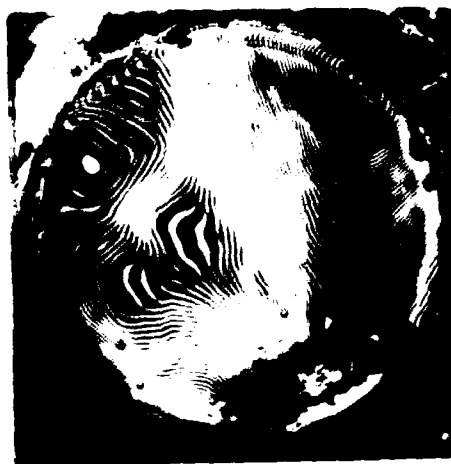
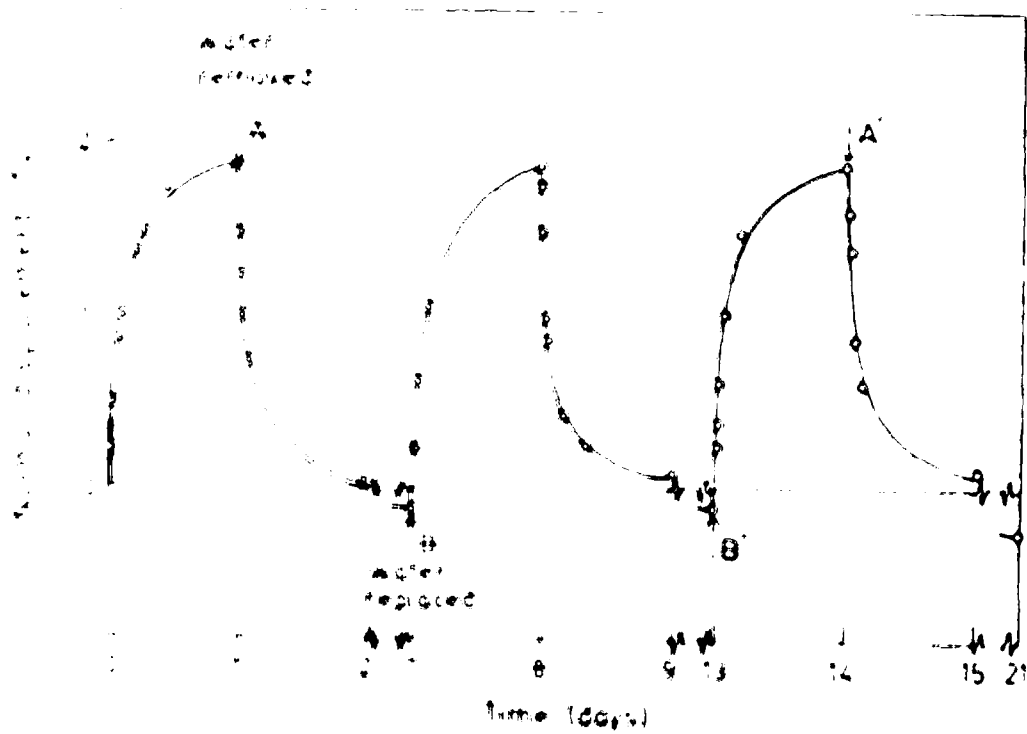


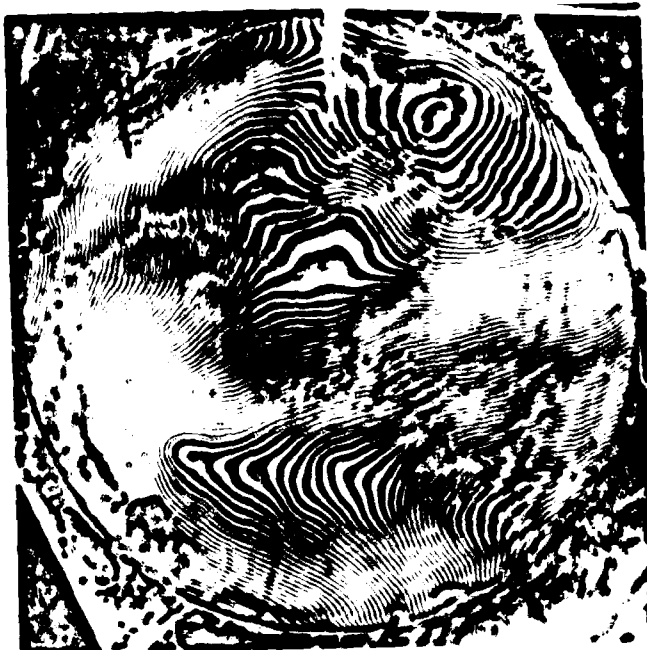
Figure 6

Figure 7

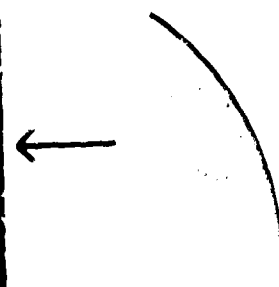


The graph shows the relationship between 'Meter Deflection' (Y-axis) and 'Time (Secs)' (X-axis). The X-axis is marked with values 0, 5, 10, 15, and 20. The Y-axis is marked with values from 0 to 100 in increments of 1. Three distinct curves are shown, each starting with a sharp rise followed by a gradual decay. The curves are labeled 'A' and 'B'. A legend indicates that the data points are 'Meter Deflection' (represented by dots) and 'Time (Secs)' (represented by crosses). The curves show a peak followed by a decay, with the peak occurring at approximately 10 seconds for curve A and 15 seconds for curve B.

(A)



(B)



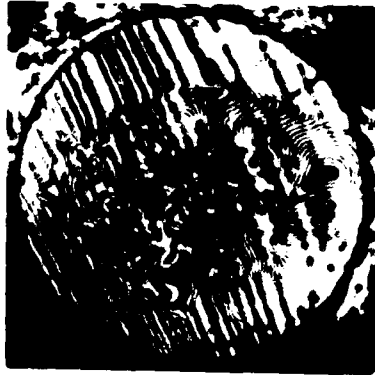
21. (A) Moiré fringes formed between two photographs taken at points indicated as A and A' in Figure 2. (B) Moiré fringes formed between photographs taken at points indicated as B and B' in Figure 2.



1:0



1:40 Mrs



1:200 Mrs

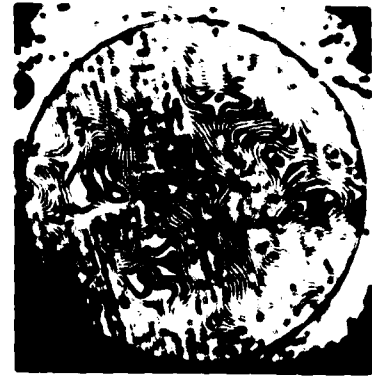
(A)



1:200 Mrs



1:200 Mrs



1:720 Mrs

(B)

22. Sequence of interference at 1:200 Mrs for a series of 1000 exposures.
 (1) Immersed in distilled water at 40°C and (2) exposed to dry air at
 40°C. The arrow indicates the onset of boiling.



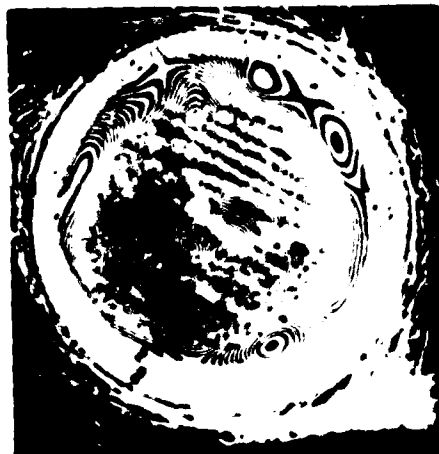
6 hrs



192 hrs



2 hrs



76 hrs

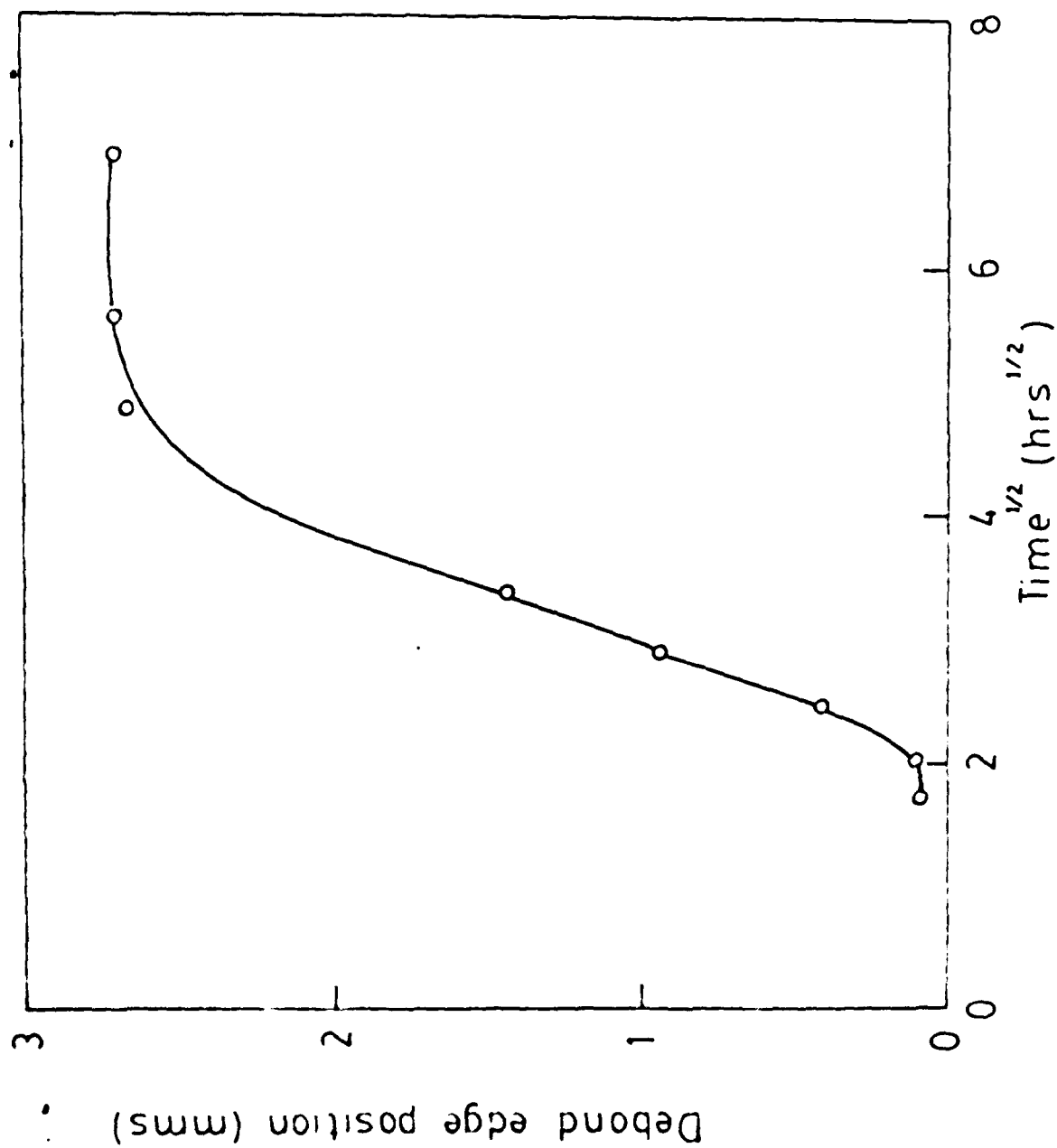


1/2 hr



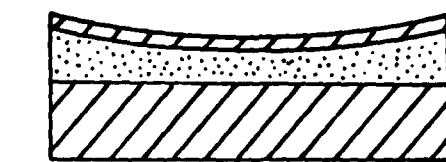
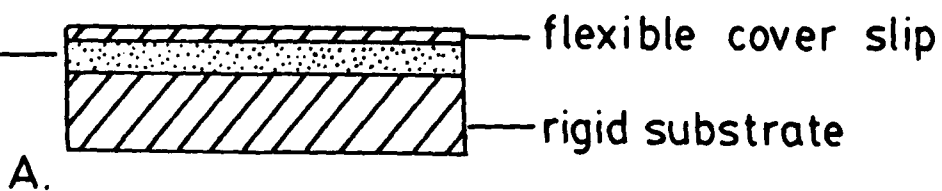
23 hrs

23. Sequence of interference photographs for a 1000 specimen inverted

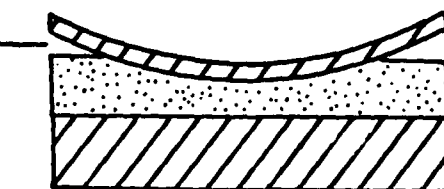


24. Graph of the position of the debonding edge at $t_{1/2}$ the cover slip/adhesive interface plotted as a function of time^{1/2} for the specimen shown in Figure 23

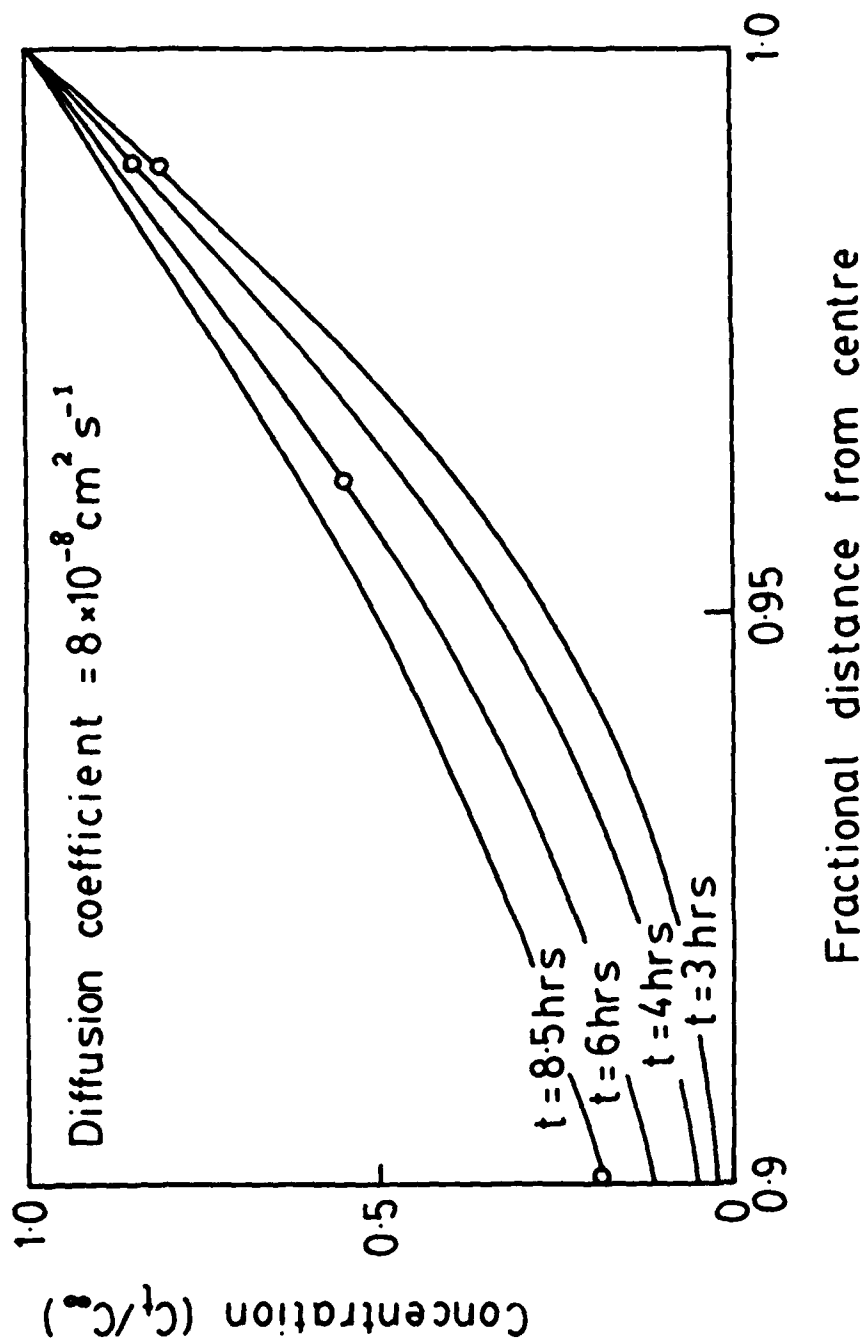
adhesive
film



debonding



25. Schematic diagram to illustrate the changing geometry of the cover slip during swelling of the adhesive in a joint exposed to an aqueous environment. Debonding follows saturation of swelling at the rim of the joint



26. Graph of the predicted water concentration (C_t/C_∞) as a function of fractional distance from the centre of the specimen. O, points representing critical concentrations for positions corresponding to the debonding edge shown in Figure 25. After Kinloch.

DATE
ILMEI
—8